Available online at www.humg.edu.vn

ESASGD 2016

GIS-IDEAS (2016)

Conference Title: International Conference on GeoInformatics for Spatial-Infrastructure Development in Earth & Allied Sciences (GIS-IDEAS)

Inudation extent and flood frequency mapping of Cuu long rivers delta using multi-temporal ERS-2 data

Nguyen Van Trung[a,*]

[a] *University of Mining and Geology, 18 Vien St, Duc Thang Ward, Bac Tu Liem District, Hanoi City 1000000, Vietnam*

Abstract

The floodplain area is largely influenced by the fluctuation of water level and seasonal change at Cuu Long rivers Delta. In the wet season, the delta landform and vegetated areas are covered with water, and vice versa in the dry season. Those land cover changes provides significant information required for mitigating the impact of climate change and sea level rise, and sustainable development. The achievement of radar systems for detecting wetlands during the wet season is to provide the land cover changes corresponding with backscattering coefficient value changes. We used serial ERS-2 data with 35 days interval during 1997 – 1998 periods to estimate the areal variation of vegetated area during the annual flood pulse. The advantage of this study is that land cover information can be observed from radar data instead of optical data due to weather condition, and able to detect the surface condition changes beneath the canopy of vegetation. The purpose of paper aims to monitor the vegetated change based on the backscattering coefficient values change while the floodwater level varies. The primary results indicate that the backscattering coefficient values decrease when the water level values increase. However, the backscattering coefficient values change at the cultivation areas is due to local flooding and faming calendar in agriculture.

Keywords: Cuu Long rivers, Land cover, ERS-2, floodplain, monitoring;

1. Introduction

Wetlands have great significance to ecosystems, particularly in the tropics where floods occur during the wet season (Ben, 2011). The lower Mekong River basin is one of the largest wetland ecosystems in Southeast Asia. The main part of this wetland is Cuu Long rivers Delta, which includes nine rivers flowing to the sea (Fig. 1a). In the wet season, floodwater flows from upper Mekong River basin into Cuu Long rivers Delta because of heavy rainfall. Conversely, the slow release of floodwaters from Cuu Long rivers Delta is a very important source of water for cultivation during the dry season.

It is important to understand the flood dynamics of the Cuu Long rivers Delta ecosystem to balance economic growth and poverty reduction with ecosystem health in a developing country, Vietnam (Kummu and Sarkkula, 2008). The species diversity of animals and plants and their ecology in the Cuu Long rivers floodplain depend on potential changes in hydrology (Campbell et al., 2006). Information about the changes in vegetated types and soil conditions at the floodplain area due to flooding is important for agriculture, pisciculture, sylviculture, and conservation. To monitor land cover changes, the relationships between vegetation types and flood dynamics during both dry and wet seasons need to be considered. Although flooding is an annual event in the floodplain, the range of flooding greatly varies from year to year. It is not possible to construct a model from a digital elevation model and land cover classification model, because the published local digital elevation model and land cover classification map are not precise enough nor sufficiently up-to-date to accommodate the

* Corresponding author. Tel.: +84-043-838-7987.
E-mail address: nguyenvantrung@humg.edu.vn.

annual flooding pattern. However, a time series of remotely sensed data could potentially be used to study floodplain vegetation dynamics and the impacts of flooding on local residents.

Several studies have been performed in the Tonle Sap floodplain area based on both synthetic aperture radar (SAR) and optical systems. Wetland ecosystems in the northwestern Tonle Sap basin were mapped and assessed with multi-polarization AIRSAR data to produce a map of fourteen land cover classes in (Milne and Tapley, 2004). Radar systems have been widely used to characterize changes in wetlands due to their weather-independent imaging capabilities. Furthermore, SAR data are sensitive to biomass, the structure of flooded vegetation, and soil moisture (Hess et al., 1995; Bouvet and Toan, 2011; Prakash, 2012). The relationship between radar signals and floodplain vegetation has been modeled using backscattering coefficients (Ulaby et al., 1990; Wang, 1995). Previous reviews (Hess et al., 1995; Schmullius,1997) have discussed the effects of radar parameters such as incidence angle, polarization, and frequency on the detection of flooding beneath a forest canopy. Those papers revealed the complexity of the relationships between radar signals and wetlands caused by the structure and density of the vegetation, the observation wavelength, and incidence angle. Backscattering at the C-band is enhanced in a floodplain due to the double bounce of the radar signal between grass or rice and water surfaces beneath the leaves (Kasischke et al., 1997) the double bounce also allows accurate measurements of water level (Alsdorf et al., 2000). An incidence angle from 20º to 30º is preferable for flooded vegetation studies, because some vegetation types exhibit bright returns that are weaker at higher incidence angles (Lang et al., 2008). Martin-Cardona et al., 2010 used Envisat ASAR C-band polarimetric, multi-incidence angle and multi-temporal characterization of Doñana wetland for flood extent monitoring. These previous studies highlighted the potential of SAR systems to detect flooding and monitor the extent of flooding during the rainy season. A major advantage of using SAR data is that it is possible to determine changes based on backscattering coefficients.

Our aim in this paper was to monitor changes in vegetation classes in the Cuu Long rivers floodplain using ERS-2 data. We performed backscattering temporal characterization of ERS-2 with VV polarizations to determine the extent of flooding in marshes based on the interaction between radar signals and wetland.

2. Study area and data

2.1. Study area

Our study area was the Vinh Long province and a part of Tra Vinh province as denoted by the covered ERS-2 SAR data acquired on January 25, 1998 in Fig. 1b. The bright areas correspond to vegetation area located in upland areas, whereas the dark areas represent objects in lowland areas such as soil and rocks, grass fields, rice paddies, settlements, etc inundated by flooding water. The topographic slope is gentle and includes various vegetation types. The topography of this area is shown as a digital terrain map (DTM) in Fig. 2b, and the topography generally follows the shape of floodplain. The land cover classes in this floodplain area change rapidly according to changes in water level. More than 30 land cover classes are present in the land use map (hereafter referred to as “the land use map 2010”) published by General Department of Land Administration, MONRE (Fig. 2a). Based on this map and digital terrain model, data for vegetation class was collected to account for the effects of water level. First, the habitat location (lowland or upland) of the selected vegetation class was considered. Changes in this vegetation class due to fluctuations in water level are very clear because water levels in this area change rapidly during the wet season. Lowland vegetations and agricultural crops locate in the habitat elevation zone from 0 to 1 m amsl, and in this zone, the tree is easily affect by flooding. The second group, located in the uplands (above 1 m amsl), comprises upland vegetation. Flooding affects only groups in this area during flood crests. Upland vegetations are strongly affected by floods during which the water level reaches the maximal flooding level. Agricultural fields refer mainly to rice paddy fields that are located in the margin of the study area. Agricultural fields are influenced not only by water level changes in the floodplain, but also by local flooding, crop cycle growth, and other related factors.

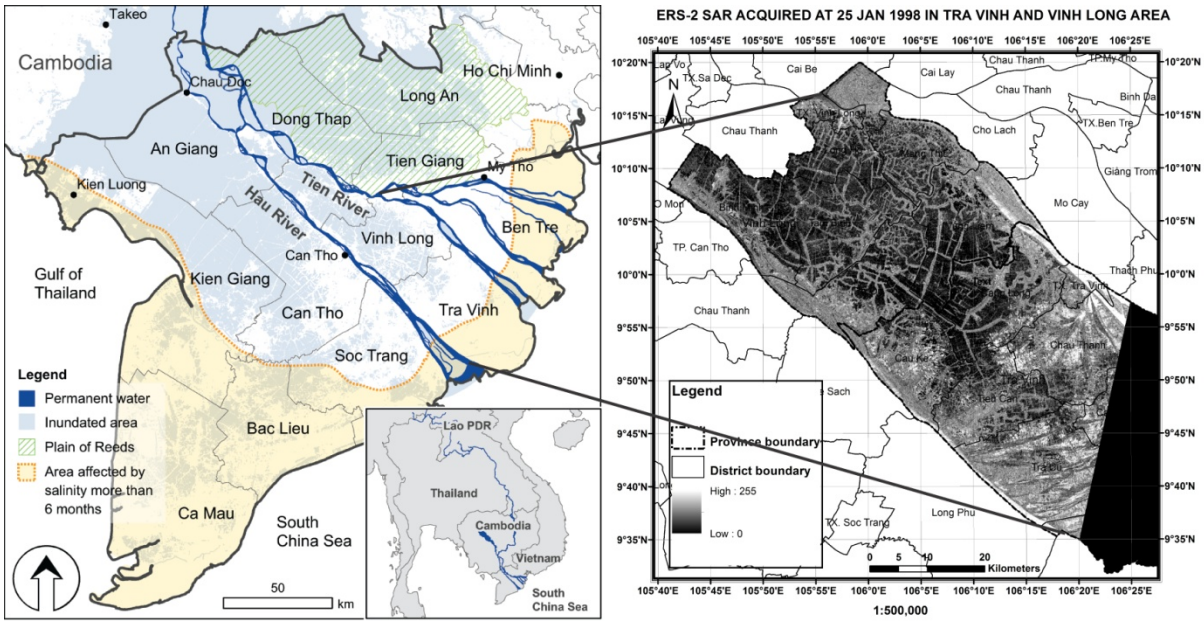

Fig. 1. (a) Map of Mekong Delta with provinces, flood-prone areas, and brackish areas (Mira, 2008);
(b) ERS-2 SAR data acquired on January 25, 1998 of study area.

2.2. Experimental Data

The data used in this study included eleven ERS-2 SAR scenes acquired from December 1997 to December 1998 (Table 1). All images were observed with a 23^0 off-nadir angle in ascending mode with VV single polarization (20 m resolution) acquired during dry and wet season of year. Surface change conditions during the wet season are much more complicated than those in the dry season (Almeia-Filho et al., 2009). ERS-2 SAR data can be used to detect changes in a 35-day interval during both dry and wet seasons. We used the time series of ERS-2 SAR data to determine backscattering coefficients of land cover classes to assess changes in land cover classes caused by flood dynamics.

Table 1. Eleven ERS-2 SAR acquisition dates and water levels measured at Dai Ngai, Tra Vinh, Can Tho, Cho Lach and My Thuan station.

No.	Date (dd mmm.yyyy)	Water level at Dai Ngai (cm)	Water level at Tra Vinh(cm)	Water level at Can Tho (cm)	Water level at Cho Lach (cm)	Water level at My Thuan (cm)
1	21 Dec.1997	9	5	5	20	32
2	25 Jan.1998	28	34	34	48	53
3	01 Mar.1998	29	31	31	48	49
4	05 Apr.1998	1	1	1	16	21
5	10 May.1998	-1	0	0	13	17
6	14 Jun.1998	-4	-5	-5	8	19
7	19 Jul.1998	-10	-19	-19	7	28
8	23 Aug.1998	14	2	2	33	58
9	27 Sep.1998	30	22	22	45	73
10	01 Nov.1998	30	23	23	47	69
11	06 Dec.1998	49	48	48	75	92

2.3. Additional Data

The water levels at acquired time of ERS-2 data recorded at Dai Ngai, Tra Vinh, Can Tho, Cho Lach, and My Thuan station, were measured as above mean sea level in Ha Tien, Vietnam, using a precise levelling from Ha Tien to Dai Ngai, realized in 2001 (MRC) (Fig. 2b). The DTM of the Tra Vinh and Vinh Long region (Fig. 2b) was generated by the MRC Technical Support Division from elevation contours with 1 meter vertical intervals of the topographic map at an original scale of 1:40 000. The calculated horizontal accuracy of the source data provided by MRC is about 65 m, and the estimated vertical accuracy of the source data is about 1 m.

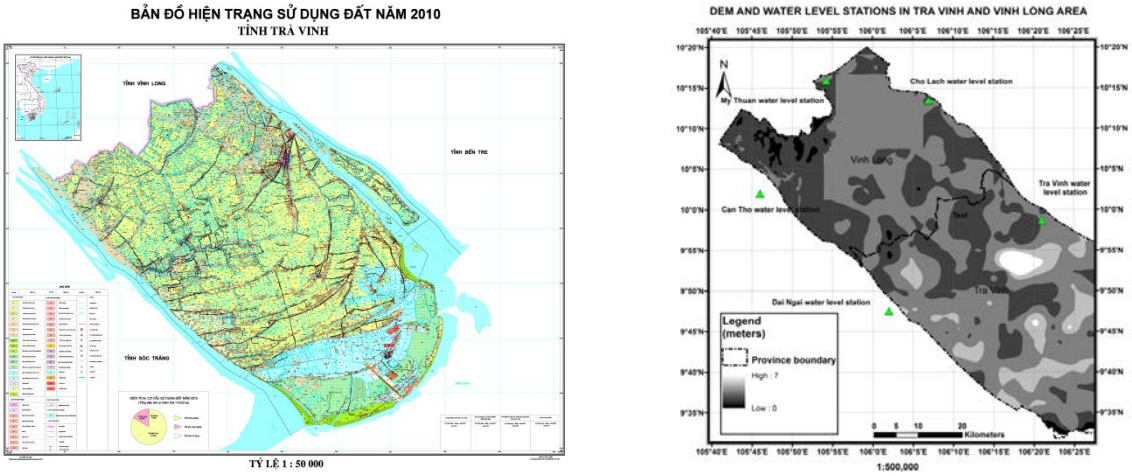

(a) (b)

Fig. 2. (a) Land use map (Source: General Department of Land Administration, MONRE); (b) DEM and water level stations (Source: MRC)

3. Methodology

3.1. ERS-2 SAR processing

All ERS-2 SAR data provided by the European Space Agency as raw data were processed to generate single look complex (SLC) data. To calculate the radar backscattering coefficient sigma nought (σ^o), the following expression was applied to each image pixel (Laur et al., 2004):

$$\sigma^0 = \left(\frac{1}{N} \cdot \sum_{i,j=1}^{i,j=N} DN_{ij}^2 \right) \cdot \frac{1}{K} \cdot \frac{\sin \alpha}{\sin \alpha_{ref}} \qquad (1)$$

where

- N is the number of pixels within the Area Of Interest (AOI) i.e. the group of pixels corresponding to the distributed target in the image,
- i and j are the range and azimuth locations of the pixels within the distributed target containing N pixels,
- DN_{ij} is the digital number corresponding to the pixel at location (i,j),
- α is the average incidence angle within the distributed target,
- α_{ref} is the reference incidence angle, i.e. 23.0 degrees.

In the present study, the sigma nought in (1) was used to calibrate the radiometric ERS-2 SAR of the Tra Vinh and Vinh Long floodplain. Geometric correction determines the accurate location of a pixel in a SAR image, i.e. the geodetic latitude and longitude. To perform this correction, the Shuttle Radar Topography Mission (SRTM) Digital Elevation Model (DEM) and a higher resolution auxiliary local DTM were used to remove terrain effect error, and each pixel was projected to a resolution of 20 m. The backscattering coefficient for each land cover type was not homogeneous due to speckle noise. To reduce this noise, a Lee filter method with sliding windows (5x5pixels) was applied to produce a mean backscattering coefficient within a homogeneous land cover class.

3.2. Object-oriented classification for land cover classes

The process of the object-oriented classification can be divided into the following steps:

- Multi-resolution segmentation,
- formulation of class hierarchy,
- decision tree-like classification (classification rules) and
- classification evaluation.

The object-oriented classification conducted using eCognition software (Baatz et al., 2004) has previously been described (Whiteside and Ahmad, 2004). The process can be split into two steps, segmentation and classification.

Multi-scale segmentation:

The object-oriented approach first involved the segmentation of image data into objects on two scale levels. The subset images were segmented into object primitives or segments using eCognition. The segmentation of

the images into object primitives is influenced by three parameters: scale, colour and form (Willhauck et al., 2000).

The scale parameter set by the operator is influenced by the heterogeneity of the pixels. The colour parameter balances the homogeneity of a segment's colour with the homogeneity of its shape. The form parameter is a balance between the smoothness of a segment's border and its compactness. The weighting of these parameters establishes the homogeneity criterion for the object primitives. A visual inspection of the objects resulting from variations in the weightings was used to determine the overall values for the parameter weighting at each scale level (Table 2).

Table 2. The overall values for the parameter weighting at each scale level.

Scale level	Scale parameter	Shape factor	Compactness	Smoothness
2	10	0.4	0.7	0.3
1	5	0.2	0.7	0.3

Classification:

Sample objects were selected as representative of land cover classes. A total of ten land cover classes for the study area were identified based on the structural formation of the vegetation and characteristic water. Class rules for the objects were then developed using spectral signatures, shape, location and the contextual relationships of the objects. These rules were then used as a basis for classification of the image, DEM and water level as shown in Table. 3. Samples for each class were selected from the image objects to act as training areas for the classification. Objects were assigned class rules using spectral signatures, shape and contextual relationships. The rules were then used as a basis for the fuzzy classification of the data with the most probable/likely class being assigned to each object.

Table 3. Construction of rule set for ERS-2 SAR based on DEM and water level data.

Land cover class	Classification rule		
	ERS-2 SAR (dB)	DEM (m)	Water level (cm)
Water	< -13	< 1	> 0
Vegetation	> -10	> 0	-
Flooded vegetation	< -10 and > -13	< 2 and > 0	<30 and >-20

4. Results and discussion

4.1. Backscattering coefficient characteristics of Land cover types

The backscattering coefficients observed for the ROIs revealed that changes in land cover types were highly correlated with changes in water levels as shown in Fig. 3. The vegetations located in the lowland were influenced earlier by floods than those in the uplands because of their low elevation - below 1 m amsl. During flooding, the surface changed due to the wet conditions. The variation in backscattering coefficients measured during both dry and wet seasons clearly accounted for such changes. According to the backscattering coefficient variation, the annual variation could be divided into the following two stages (Fig. 3a):

- The dry season stage (water level ranged below 0.3 m amsl) was characterized by a stable period in terms of C-band backscattering. During this period, the surface water in the floodplain gradually started to disappear. The backscattering coefficient decreased in range from 4 to 8 dB because the water level dropped to a minimum, which in turn resulted in the double bound diminishing to a minimum in the dry season. The distinction among backscattering coefficients of vegetation, flooded vegetation and water types was clear.

- The wet season stage (water level increased above 0.3 m amsl) corresponded to a rapid decrease in the backscattering coefficients. Because the water level reached the leaf canopy or fully inundated the vegetation, the water surface reflection increased, resulting in a decrease in the total backscatter. The backscattering coefficients of lowland grasses and agricultural tree were always the lowest when the water level exceeded their height so that lowland vegetation areas were progressively replaced by floodwater surface areas during this flood stage, which corresponded to a decrease in the backscattering coefficients. In particular, upland fruit trees with the highest trees were not often fully inundated, leading to the highest backscattering coefficients in this stage, partially due to double bounce.

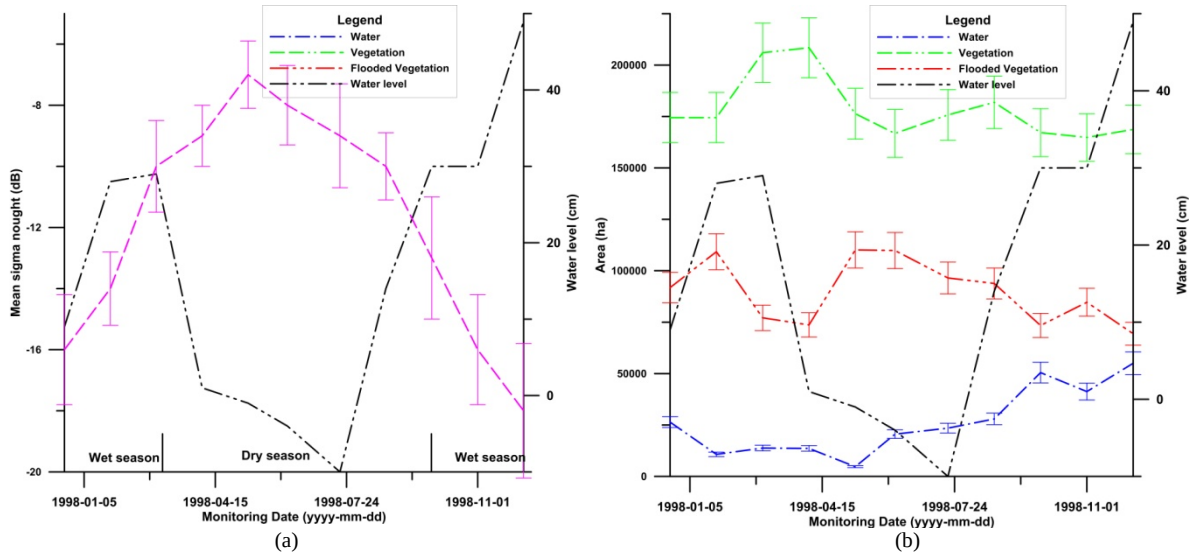

Fig. 3. (a) Water level and backscattering coefficient of vegetation class during year ; (b) Land cover classes area change in the study area.

The backscattering coefficients of lowland vegetation decreased from -7.6 dB in the dry season to -12.9 dB in the wet season. During the dry season, the difference in backscattering coefficients between flooded vegetation and vegetation was about 4.2 dB. The maximum backscattering coefficients difference in lowland vegetation between the two seasons was about 5.1 dB. This accounts for the different backscattering mechanisms observed: double bounce, volume and surface scattering. As the water level increased, backscattering decreased in all cases because of specular scattering. However, double bounce increased, particularly in the lowland fruit trees, which resulted in a minimal decrease in backscattering coefficients during the wet season. In contrast, the increased water level and wet soil contributed to a loss in backscattered radar power due to increased specular scattering for lowland vegetations during the wet season. A tree with a thick trunk plays an important role in double bounce backscattering when the ground surface is submerged by floodwater (Lee et al., 2004). However, the thin trunk of a fruit tree does not contribute much to double bounce backscattering.

Upland vegetation and agricultural areas were located in topographically high regions, above 1 m amsl. The land cover changes in these areas were more affected by near-crest flooding. The backscattering coefficients of vegetation type also had different patterns of variation during each of the two water level variation stages, as shown in Fig. 3. The backscattering coefficient of the upland vegetation was always higher than that of lowland vegetation. The maximum and minimum backscattering coefficients of the upland vegetation during the observation time were about -7.1 dB and -13.2 dB, respectively. As shown in Fig. 3, the upland vegetations were affected by flooding at about 1 m amsl, while lowland vegetations were affected by a flood level of about 0.3 m amsl. It is worthy to note that the radar backscattering values for upland fruit trees were relatively high because of double bounce, even during the peak of a flood. When the water level was below 1 m amsl, the grasses in the two areas had different values. This result implies that C-band radar backscattering from a grassy area is directly governed by soil water content, while C-band radar backscattering from forests or fruit trees has a more complicated pattern when surface water is present due to a more complicated scattering mechanism. The agricultural areas showed a very similar pattern of variation to the upland grasses in terms of backscattering coefficients for water levels higher than 1 m amsl. During the dry season, the agricultural fields had lower backscattering coefficients than the natural grasslands. This can be explained by the difference in biomass between these two vegetation types, as shown in Fig. 4. Short vegetation is sensitive to surface conditions during the dry season. Cultivation, harvesting, and growth also cause large changes in agricultural areas (Toan et al., 1997). Therefore, it is difficult to make a direct comparison between agricultural areas and natural grasslands using only backscattering coefficients. All vegetation types except lowland forests showed steeper negative slopes of backscattering coefficients during the early-wet season stage and slightly less steep positive slopes during the late-wet season stage. This may be associated with the flooding pattern in this area; flooding involved rapid changes in surface conditions, but gradual recovery as the water receded.

4.2. Land cover variation with respect to water level

We calculated and plotted the areal variation of vegetation and flooded vegetation types and water-covered surfaces Fig. 3b. with error bars of ± 1 standard deviation. The vegetation area was reduced to 20.9% of the total vegetation area when the water level reached its peak (0.48 m amsl), which indicates that about 15.1% of the total study area was affected by flooding.

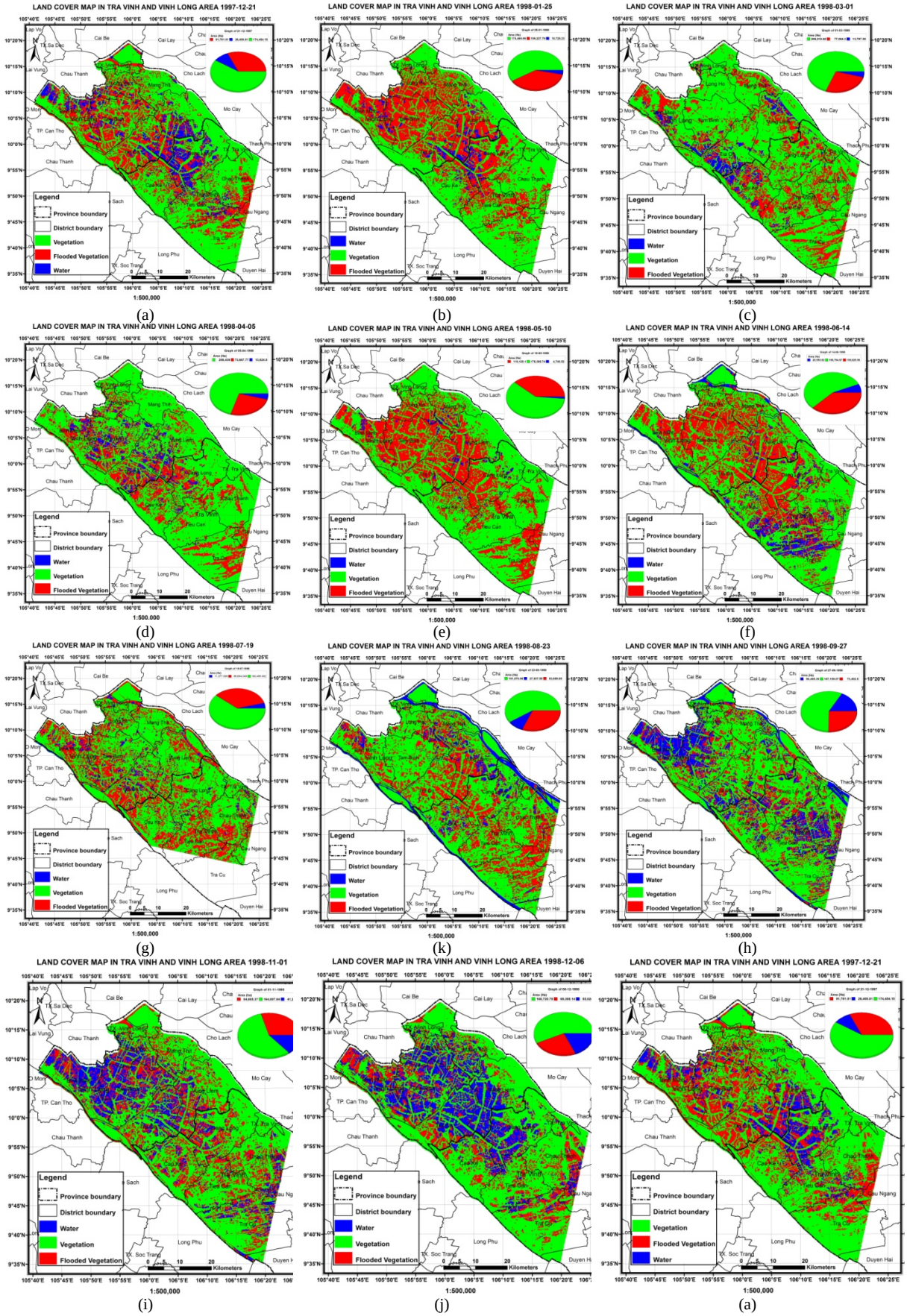

Fig. 4. Land cover map of (a) 1997-12-21; (b) 1998-01-25; (c) 1998-03-01; (d) 1998-04-05; (e) 1998-05-10; (f) 1998-06-14; (g) 1998-07-19; (k) 1998-08-23; (h) 1998-09-27; (i) 1998-11-01; and (j) 1998-12-06 in the study area.

For the vegetation area dominated the entire area whereas the flooded vegetation covered a smaller area. The maximum flooded vegetation area comprised about 37.8% of the total study area. In the crest flooding, the

minimum areal flooded vegetation was 23.6% of the total study area at a water level of 0.48 m amsl. This indicates that the flooded vegetation area (about 14.2% the total study area) was converted to vegetation area when the water level decreased.

The total area of water surface was only 1.6% of the total study area at dry season. However, this increased 18.7% of the total study area at wet season. The areal variation of vegetation was very sensitive to fluctuations in water level because of the low height of the grasses and agricultural tree. After crest flooding, areal flooded vegetation and areal vegetation were decreased rapidly meanwhile the area of water surface increased. This means that areal flooded vegetation and areal vegetation were transferred to area of water surface.

These maps provide detailed views of each land cover class over time, thereby providing insight into the changes in all land cover classes during a flood pulse. Since the flooding starts from the water level above 0.3 m amsl, we examined the land cover at 0.3 m amsl. A land cover map at 0.3 m amsl within the flood development stage was generated by simple simulation using the DTM map, the land use map, and the water level record at 0.3m. The land cover results extracted from ERS-2 SAR and DTM and land use map results at water level 0.3 m were generally similar, with differences ranging from 0 to 12.5% of the total land cover class area. The areal difference for vegetation was about 0.3% of the total land area. The differences, however, were particularly high for flooded vegetation, water surface about 3.8% and 1.2% of the total land cover area, respectively. There are several potential error sources in the simple estimation derived from the DTM and land use map. For instance, the elevation accuracy of DTM data is about 1 m and the height accuracy of vegetation is about 0.5 meters. Thus, the results derived from the DTM and land use map are not accurate for larger areas with abundant trees of various heights. Together, our results indicate that land cover variations that take water level into account can increase our understanding of flood dynamics and help manage human activity and floods in wetland areas.

5. Conclusions

In this study, we studied changes in land cover classes in the Tonle Sap floodplain using ERS-2 SAR data, and a land cover area variation were established as a water level change. The results indicate that backscattering coefficient changes measured for land cover classes between dry and wet seasons depended on location, characteristics of the vegetation, and water level changes.

When we computed the area changes of vegetation type, we found that the area changes depended on the interaction between water level and vegetation height at various elevations. The total area of vegetation was the largest among the land cover classes at about 70.4% of the study area, and the effect of flooding on this area was strong. A backscattering coefficient change from -7.6 dB to -20.6 dB for vegetation in the flood development stage corresponded to an areal percentage change of vegetation about 15.1% of the total study area according to our calculation. The flooded vegetation area (about 14.2% of total study area) was converted to vegetation area when the water level decreased after the crest flooding. The computed results also revealed that a large portion of land cover classes (about 17.1% of total study area) was covered with water at the peak of flooding. When we compared results extracted from ERS-2 SAR data and those obtained from a DTM and land use map at 0.3 m amsl, we found an areal difference in land cover classes with a maximum of 3.8% in the flooded vegetation. It indicates that it is necessary to use SAR data for future flood management.

Acknowledgements

The ERS-2 SAR data were provided by the European Space Agency to N. V. Trung as a Category-1 project (PI No. 19170). Author would appreciate Mekong River Commission (MRC) for providing water level data and the digital terrain model. Author also thanks General Department of Land Administration, MONRE for the land use map.

References

Almeia-Filho, R., Y. E. Shimabukuro, A. Rosenqvist and G. A. Sanchez, 2009.“Using dual-polarized ALOS PALSAR data for detecting new fronts of deforestation in the Brazilian Amazonia,” *Int. J Remote Sens*., vol. 30, no. 14, pp. 3735-3742.

Alsdorf, D. E., J. M. Melack, T. Dunne, L. A. K. Mertes, L. L. Hess, and L. C. Smith, 2000.“Interferometric radar measurements of water level changes on the Amazon flood plain,” *Nature*, vol. 404, pp. 174-177.

Baatz, M., Benz, U., Dehghani, S., Heynen, M., Höltje, A., Hofmann, P., Lingenfelder, I., Mimler, M., Sohlbach, M., Weber, M., & Willhauck, G., (2004), eCognition Professional: User guide 4.; Munich: Definiens-Imaging.

Ben, A. L., 2011. *Wetlands: Integrating Multidisciplinary Concepts.* NewYork, USA: Springer, ch. 1, pp 3-25.

Bouvet, A., and T. Le Toan, 2011.“Use ENVISAT/ASAR wide-swath data for timely rice fields mapping in the Mekong River Delta,” *Remote Sens. Environ.*, vol. 115, no. 4, pp. 1090-1101.

Campbell, I. C., C. Poole, W. Giesen, and J. Valbo-Jorgensen, 2006.“Species diversity and ecology of Tonle Sap Great Lake, Cambodia,” *Aquat. Sci*., vol. 68, no. 3, pp. 355-373.

Hess, L., J. Melack, S. Filoso, and Y. Wang, 1995.“Delineation of inundated area and vegetation along the Amazon floodplain with the SIR-C synthetic aperture radar,” *IEEE Trans. Geosci. Remote Sensing*, vol. 33, no. 4, pp. 896−904.

Kasischke, E., and L. Bourgeau-Chavez, 1997.“Monitoring South Florida Wetlands Using *ERS*-1 SAR Imagery,” *Photogramm. Eng. Remote Sens.*, vol. 63, no. 3, pp. 281-291.

Kummu, M., and J. Sarkkula, 2008.“Impact of the Mekong River flow alteration on the Tonle Sap flood pulse,” *A Journal of the Human Environment*,vol.37, no. 3, pp. 185−192.

Lang, M. W., P. Townsend, and E. Kasischke, 2008.”Influence of incidence angle on detecting flooded forests using C-HH synthetic aperture radar data,” *Remote Sens. Environ.*, vol. 112, no. 10, pp. 3898−3907.

Laur, H., P. Bally , P. Meadows , J. Sanchez , B. Schaettler , E. Lopinto , D. Esteban , 2004. “Derivation of the backscattering coefficient σ^o in ESA ERS SAR PRI products,” Issue 2, Rev. 5f , ESA, pp 4-5.

Lee, S. K., S. H. Hong, S. W. Kim, Y. Yamaguchi, and J. S. Won, 2006.“Polarimetric features of oyster farm observed by AIRSAR and JERS-1,” *IEEE Trans. Geosci. Remote Sens.*, vol. 44, no. 10, pp. 2728-2735.

Marti-Cardona, B., C. Lopez-Martinez, J. Dolz-Ripolles, and E. Bladè-Castelle, 2010.“ASAR polarimetric, multi-incidence angle and multitemporal characterization of Doñana wetlands for flood extent monitoring,” *Remote Sens. Environ.*, vol. 114, no. 11, pp. 2802-2815.

Milne, A. K., and I. J. Tapley, 2004.“Mapping and assessment of wetland ecosystems in the northwestern Tonle Sap Basin with AIRSAR Data,” Mekong River Commission and the University of New South Wales (*project report*), 129 pages.

Mira K., 2008. “Mekong Delta at the Crossroads: More Control or Adaptation?” *Ambio*, Vol. 37, No. 3,pp 205-212.

Prakash, R., D. Singh, and N. P. Pathak, 2012.“A fusion approach to retrieve soil moisture with SAR and optical data,” *IEEE J. Sel. Topics Appl. Earth Observ. Remote Sens. (JSTARS)*, vol. 5, no. 1, pp. 196-206.

Schmullius, C., and D. Evans, 1997.“Review article synthetic aperture radar (SAR) frequency and polarization requirements for applications in ecology, geology, hydrology, and oceanography: A tabular status quo after SIR-C/X-SAR,” *Int. J. Remote Sens.*, vol. 18, no. 13, pp. 2713−2722.

Toan, T. L., F. Ribbes, L. F. Wange, N. Floury, N. Ding, and K. H. Kong, 1997.“Rice crop mapping and monitoring using ERS-1 data based on experiment and modeling results,” *IEEE Trans. Geosci. Remote Sensing*, vol. 35, no. 1, pp. 41−56.

Ulaby, F. T., K. Sarabandi, K. McDonald, M. Whitt, and M. C. Dobson, 1990.“Michigan microwave canopy scattering model,” *Int. J. Remote Sens.*, vol. 11, no. 7, pp. 1223−1253.

Wang, Y., L. L. Hess, S. Filoso, and J. M. Melack, 1995.“Understanding the radar backscattering from flooded and nonflooded Amazonian forests: results from canopy backscatter modeling,” *Remote Sens. Environ.*, vol. 54, no. 3, pp. 324−332.

Whiteside, T., & Ahmad, W., 2004. “Object-oriented classification of ASTER imagery for landcover mapping in monsoonal northern Australia,” Proceedings of 12th Australasian Remote Sensing and Photogrammetry Conference.

Willhauck, G., Schneider, T., De Kok, R., & Ammer, U., 2000. “Comparison of object-oriented classification techniques and standard image analysis for the use of change detection betweeen SPOT multispectral satellite images and aerial photos,” Proceedings of XIX ISPRS Congress, 16-22 July, Amsterdam.